

Article

# Transcriptomic Immune Profiles Can Represent the Tumor Immune Microenvironment Related to the Tumor Budding Histology in Uterine Cervical Cancer

Tan Minh Le <sup>1,2</sup> , Hong Duc Thi Nguyen <sup>1,2</sup> , Eunmi Lee <sup>1,2</sup>, Donghyeon Lee <sup>1,2</sup>, Ye Seul Choi <sup>1,2</sup>, Junghwan Cho <sup>3</sup>, Nora Jee-Young Park <sup>3,4</sup>, Hyung Soo Han <sup>1,2,3,5,\*</sup>  and Gun Oh Chong <sup>3,6,\*</sup> 

<sup>1</sup> Department of Biomedical Science, Graduate School, Kyungpook National University, Daegu 41944, Korea

<sup>2</sup> BK21 Four Program, School of Medicine, Kyungpook National University, Daegu 41944, Korea

<sup>3</sup> Clinical Omics Institute, Kyungpook National University, Daegu 41405, Korea

<sup>4</sup> Department of Pathology, Kyungpook National University, Chilgok Hospital, Daegu 41404, Korea

<sup>5</sup> Department of Physiology, School of Medicine, Kyungpook National University, Daegu 41944, Korea

<sup>6</sup> Department of Obstetrics and Gynecology, Kyungpook National University, Chilgok Hospital, Daegu 41404, Korea

\* Correspondence: hshan@knu.ac.kr (H.S.H.); gochong@knu.ac.kr (G.O.C.)

**Abstract:** Tumor budding (TB) histology has become a critical biomarker for several solid cancers. Despite the accumulating evidence for the association of TB histology with poor prognosis, the biological characteristics of TB are little known about in the context related to the tumor immune microenvironment (TIME) in uterine cervical cancer (CC). Therefore, this study aimed to identify the transcriptomic immune profiles related to TB status and further provide robust medical evidence for clinical application. In our study, total RNA was extracted and sequenced from 21 CC tissue specimens. As such, 1494 differentially expressed genes (DEGs) between the high- and low-TB groups were identified by DESeq2. After intersecting the list of DEGs and public immune genes, we selected 106 immune-related DEGs. Then, hub genes were obtained using Least Absolute Shrinkage and Selection Operator regression. Finally, the correlation between the hub genes and immune cell types was analyzed and four candidate genes were identified (one upregulated (*FCGR3B*) and three downregulated (*ROBO2*, *OPRL1*, and *NR4A2*) genes). These gene expression levels were highly accurate in predicting TB status (area under the curve >80%). Interestingly, *FCGR3B* is a hub gene of several innate immune pathways; its expression significantly differed in the overall survival analysis ( $p = 0.0016$ ). In conclusion, *FCGR3B*, *ROBO2*, *OPRL1*, and *NR4A2* expression can strongly interfere with TB growth and replace TB to stratify CC patients.

**Keywords:** cervical cancer; gene expression; immune-related genes; tumor budding; tumor immune microenvironment



**Citation:** Le, T.M.; Nguyen, H.D.T.; Lee, E.; Lee, D.; Choi, Y.S.; Cho, J.; Park, N.J.-Y.; Han, H.S.; Chong, G.O. Transcriptomic Immune Profiles Can Represent the Tumor Immune Microenvironment Related to the Tumor Budding Histology in Uterine Cervical Cancer. *Genes* **2022**, *13*, 1405. <https://doi.org/10.3390/genes13081405>

Academic Editor: Gael Roue

Received: 10 July 2022

Accepted: 4 August 2022

Published: 7 August 2022

**Publisher's Note:** MDPI stays neutral with regard to jurisdictional claims in published maps and institutional affiliations.



**Copyright:** © 2022 by the authors. Licensee MDPI, Basel, Switzerland. This article is an open access article distributed under the terms and conditions of the Creative Commons Attribution (CC BY) license (<https://creativecommons.org/licenses/by/4.0/>).

## 1. Introduction

Uterine cervical cancer (CC) is one of the most common cancers in women [1]. Although progress has been made in CC prevention and management, it still has a poor outcome. According to Globocan 2020, 3218 new CC cases and 1014 CC deaths occur annually in Korea [1]. Therefore, novel markers for CC diagnosis, prognosis, and treatment have long been of great interest.

Recently, tumor budding (TB) histology has become a critical biomarker for several solid cancers, including colorectal cancer, head and neck cancer, pancreatic cancer, etc. [2–6]. In addition, we previously showed that TB status is a potential independent prognostic factor and can strongly interfere with CC treatment strategies [7]. However, the main disadvantage of this histopathological marker is that it can only be established after surgery. In this scenario, insights into the biological characteristics of TB can provide a helpful direction to investigate potential tools for CC management.

The tumor microenvironment (TME), referred to as a “house” of cancer cells, comprises non-resident components (tumor-derived cells and infiltrating leukocytes) and resident components (blood vessels, nerve fibers, mesenchyma, and structural components) [8–10]. Some researchers suggested six TME subgroups, including hypoxic niche, immune microenvironment, metabolism microenvironment, acidic niche, innervated niche, and mechanical microenvironment [8]. The tumor immune microenvironment (TIME) is an important aspect because the theory of TIME can provide a powerful account of how to develop effective anti-tumor therapies. It is revealed that the immune response in TME can sometimes block cancer development [11]. Unfortunately, in many cases, tumor cells often activate the immunosuppressive mechanisms and lead to tumor escape from the host immune response [8–10].

Until now, TB has been little known in relation to the TIME. Nearchou (2019) and Dawson (2020) found that CD8+/CD3+ T-cell location and density are correlated with TB status in colorectal cancer [12,13]. However, there have not been any published studies about the relationship between tumor buds and TIME in CC. Therefore, this study aimed to identify the transcriptomic immune profiles related to TB status and further provide robust medical evidence for clinical application, such as stratification, prognosis, and immune-targeted therapeutic strategy.

## 2. Materials and Methods

### 2.1. Sample Collection

This study was conducted between 2011 and 2018. Twenty-one tissues from early stage and locally advanced CC patients were obtained after radical hysterectomy. The exclusion criteria included a history of preoperative chemotherapy, radiotherapy, and synchronous malignancies. The 2009 International Federation of Gynecologic Obstetrics (FIGO) staging for carcinoma of the cervix was used to stage the patients [14]. The flowchart in Figure 1 represents the overall process of this study.

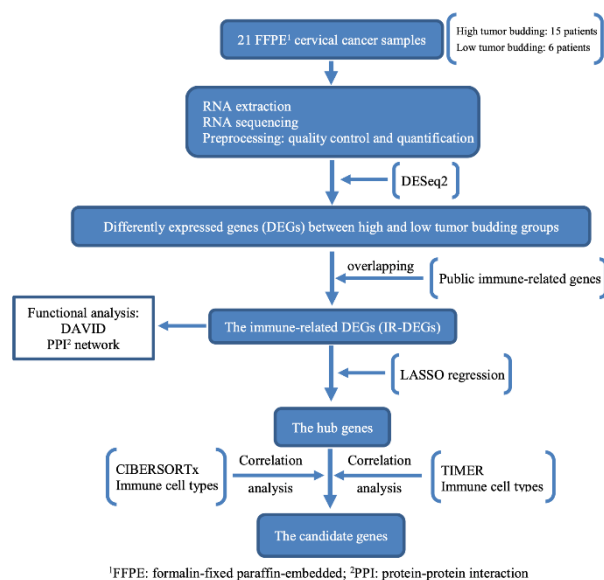


**Figure 1.** Flowchart of the study.

### 2.2. Pathological Process

Specimens were selected from the tumor area and stained with hematoxylin and eosin. All tissue slices (ranging from 8 to 25 per patient) were carefully assessed for histopathological features. TB is described as a single neoplastic cell or cell cluster of up to four neoplastic cells at the invasive front of the tumor [15]. High TB was defined as  $\geq 5$  buds/high-power field (Supplementary Figure S1). Detailed examination methods and high-TB criteria have been described previously [7,16].

### 2.3. Clinical Parameters and Follow-Up

Clinicopathological parameters included age, tumor stage (early stage < IIb and late stage  $\geq$  IIb), histological subtype, TB status (high and low), overall survival (OS), and relapse-free survival (RFS). All patients were followed-up every three months for the first two years, every six months for the next five years, and then annually [7,16].

### 2.4. RNA Extraction and Sequencing

For each patient, total RNA was extracted from 2 to 4 sections (5  $\mu$ m each) of a block using the ReliaPrep<sup>TM</sup> FFPE RNA Miniprep System (Promega, Madison, WI, USA), according to the manufacturer's protocol. Next, we conducted library preparation using the TruSeq RNA Exome Kit and RNA sequencing with NovaSeq 6000 (Illumina, San Diego, CA, USA). The quantity and quality were checked using a Qubit 4 Fluorometer (Thermo Fisher Scientific, Waltham, MA, USA), and Bioanalyzer (Agilent Technologies, Santa Clara, CA, USA).

### 2.5. Bioinformatic Analysis

Raw sequences in the FASTQ format from the sequencer were assessed for read quality using FASTQC (<https://www.bioinformatics.babraham.ac.uk/projects/fastqc/>, accessed on 8 September 2021). All low-quality reads and sequencing adapters were removed using Trimmomatic [17,18]. Kallisto was used to quantify RNA-seq data [19]. DESeq2 package was used to compare gene expression between high- and low-TB groups [20]. The  $p$  value and  $|\log_2\text{-fold-change}|$  thresholds were 0.05 and 1.0, respectively. A volcano plot of differentially expressed genes (DEGs) was created using the “ggplot2” package [21].

### 2.6. Immune-Related Gene Dataset

A list of 2483 public immune genes was downloaded from the ImmPort database (<https://www.immport.org/shared/home/>, accessed on 20 January 2022) [22]. The overlapping genes between DEGs and 2483 public immune-related genes were immune-related DEGs (IR-DEGs).

### 2.7. Functional Analysis

The IR-DEGs were uploaded to the DAVID website (<https://david.ncifcrf.gov/tools.jsp>, accessed on 19 April 2022) for analyzing the Gene Ontology (GO) and Kyoto Encyclopedia of Genes and Genomes (KEGG) pathways [23]. Benjamini-and-Hochberg-adjusted  $p < 0.05$  was considered statistically significant.

### 2.8. Immune-Cell-Type Analysis

Gene-length-normalized expression was imported into the TIMER2.0 website (<http://timer.cistrome.org/>, accessed on 21 April 2022) to estimate the proportions of different immune cell types using the TIMER (TIMER immune cells) and CIBERSORT (CIBERSORT immune cells) algorithms [24–26]. The fraction of immune cells between the high- and low-TB groups was compared using the Wilcoxon rank-sum test and a boxplot was drawn with the “ggpubr” package [27]. Benjamini-and-Hochberg-adjusted  $p < 0.05$  was considered statistically significant.

### 2.9. Candidate Gene Analysis

We performed Least Absolute Shrinkage and Selection Operator (LASSO) regression, a machine learning method in the “glmnet” package, to select hub genes from IR-DEGs [28]. Then, the correlation analysis (Spearman's method in the “corrplot” package) between the hub genes and immune cell types was used to select the significantly correlated genes [29]. The candidate genes were the overlapping genes between CIBERSORT and TIMER. The  $p$  value threshold was 0.05.

### 2.10. Protein–Protein Interaction Network Analysis

To thoroughly examine the candidate gene functions, 106 IR-DEGs were uploaded to the STRING website (version 11.5) to analyze the protein–protein interaction (PPI) (<https://string-db.org/>, accessed on 6 May 2022) [30]. The network was visualized using Cytoscape software v3.9.1 (Shannon, P et al., Institute for Systems Biology, Seattle, WA, USA) [31].

### 2.11. Receiver Operating Characteristic (ROC) Curve and Survival Analysis

The “pROC” package was used to determine the diagnostic accuracy of the candidate genes between the high- and low-TB groups in CC [32]. Next, the optimal cut-off point for survival analysis was determined using maxstat (maximally selected rank statistics) in the “survminer” package [33]. The different expression levels of candidate genes in OS and RFS were explored using the log-rank test in the “survival” package [34,35].

## 3. Results

### 3.1. Clinical Information

Twenty-one participants were enrolled. The clinicopathological information is shown in Table 1. The median age was 48 years (32–71 years). The early stage was dominant (81%). Fifteen and six patients (71.4% and 28.6%, respectively) belonged to the high- and low-TB groups, respectively. In addition, the distribution of pathological diagnoses was as follows: squamous cell carcinoma: 15 (71.4%); adenocarcinoma: 6 (23.8%); and adenosquamous cell carcinoma: 1 (4.8%).

**Table 1.** Patients’ characteristics.

|                              | (ALL)<br>N = 21 | N  |
|------------------------------|-----------------|----|
| Age (range)                  | 48 (32–71)      | 21 |
| Clinical Stage:              |                 | 21 |
| Early stage                  | 17 (81.0%)      |    |
| Late stage                   | 4 (19.0%)       |    |
| Histology:                   |                 | 21 |
| Squamous cell carcinoma      | 15 (71.4%)      |    |
| Adenocarcinoma               | 5 (23.8%)       |    |
| Adenosquamous cell carcinoma | 1 (4.8%)        |    |
| Tumor budding:               |                 | 21 |
| Low (<5 TBs <sup>1</sup> )   | 6 (28.6%)       |    |
| High (≥5 TBs)                | 15 (71.4%)      |    |

<sup>1</sup>. TBs, tumor buds.

### 3.2. Identification of IR-DEGs

The volcano plot indicates 1464 DEGs (929 upregulated and 535 downregulated genes) between the high- and low-TB groups (Figure 2 and Supplementary Table S1). Subsequently, 106 IR-DEGs that overlapped between the DEGs and immune-related gene database (Figure 3A) were selected. A heatmap was then used to visualize the hierarchical clustering of the identified IR-DEGs (Figure 3B and Supplementary Table S2).

### 3.3. Functional Enrichment Analysis

The functions of 106 IR-DEGs were investigated by GO enrichment and KEGG pathway analyses. As shown in Figure 4A and Supplementary Tables S3 and S4, the 50 most significantly enriched genes were involved in immune response (GO:0006955,  $p = 3.2 \times 10^{-16}$ ), cytokine-mediated signaling pathway (GO:0019221,  $p = 9 \times 10^{-13}$ ), Fc- $\gamma$  receptor signaling pathway involved in phagocytosis (GO:0038096,  $p = 5.3 \times 10^{-7}$ ), external side of plasma membrane (GO:0009897,  $p = 8.2 \times 10^{-13}$ ), and extracellular space (GO:0005615,  $p = 9.2 \times 10^{-11}$ ). Regarding the KEGG pathway, natural-killer-cell-mediated cytotoxicity (hsa04650,  $p = 1.47 \times 10^{-6}$ ), cytokine–cytokine receptor interaction (hsa04060,



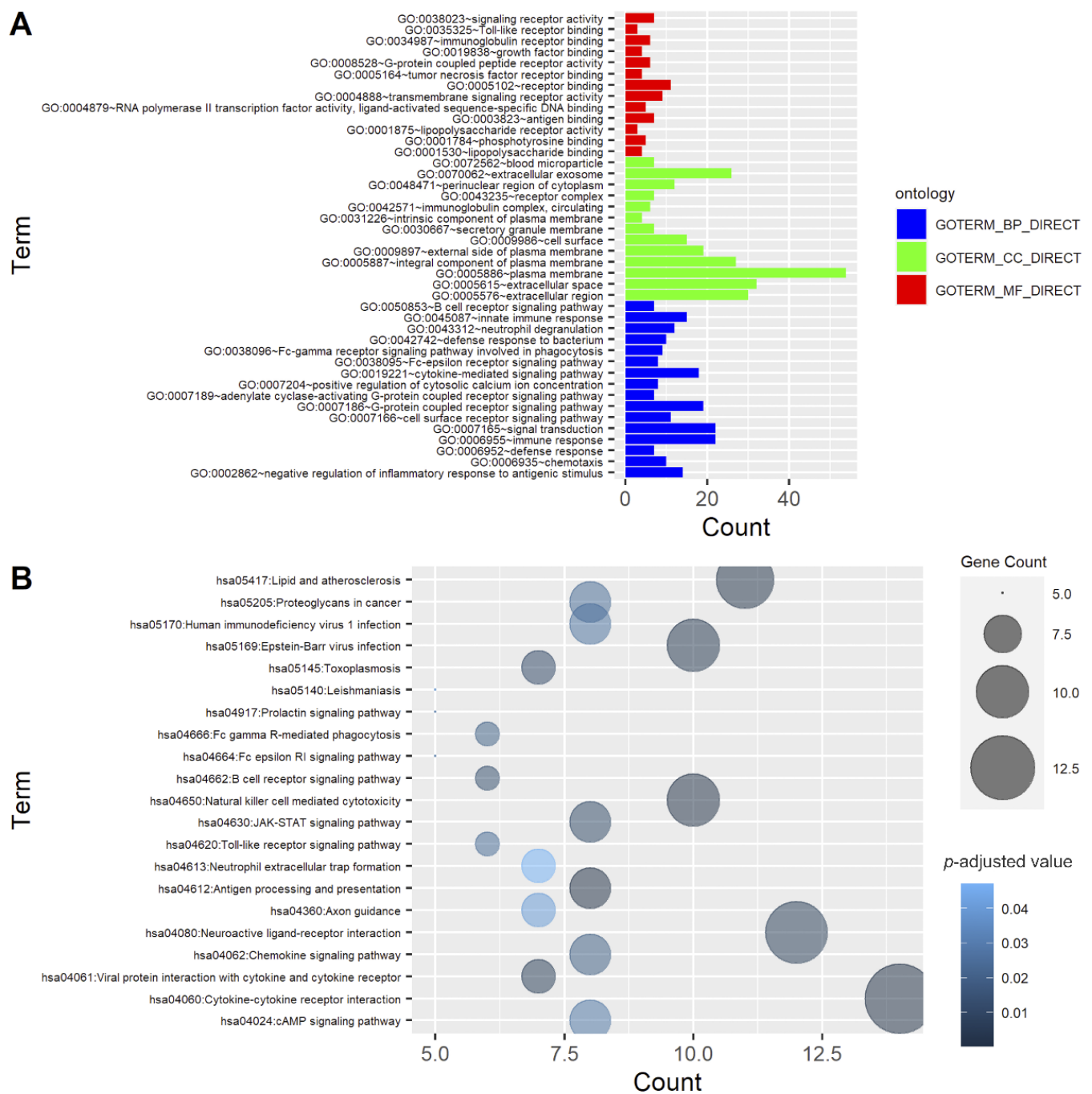


**Figure 4.** Functional enrichment analysis of 106 immune-related differentially expressed genes (IR-DEGs). **(A)** Gene Ontology (GO). The bar plot shows the top 50 enriched IR-DEGs from GO analysis. Blue, green, and red represent biological process (BP), cellular component (CC), and molecular function (MF) GO terms, respectively. **(B)** Kyoto Encyclopedia of Genes and Genomes (KEGG) pathway. Different colors and sizes of bubbles represent different  $p$  values and gene counts of a pathway.

### 3.4. Identification of Candidate Immune-Related Genes

#### 3.4.1. Selection of Hub Immune-Related Genes with LASSO Regression

LASSO regression was implemented for the 106 IR-DEGs. In total, 16 hub genes with the best lambda value, including *UNC93B1*, *ROBO2*, *RARB*, *PTH1R*, *PSMD14*, *OPRL1*, *NR4A2*, *LTBP3*, *LILRB3*, *KLRC2*, *IGLV4-60*, *IGKV3-7*, *IGHV3-35*, *FCGR3B*, *CSRP1*, and *AKT3*, were selected (Figure 5).

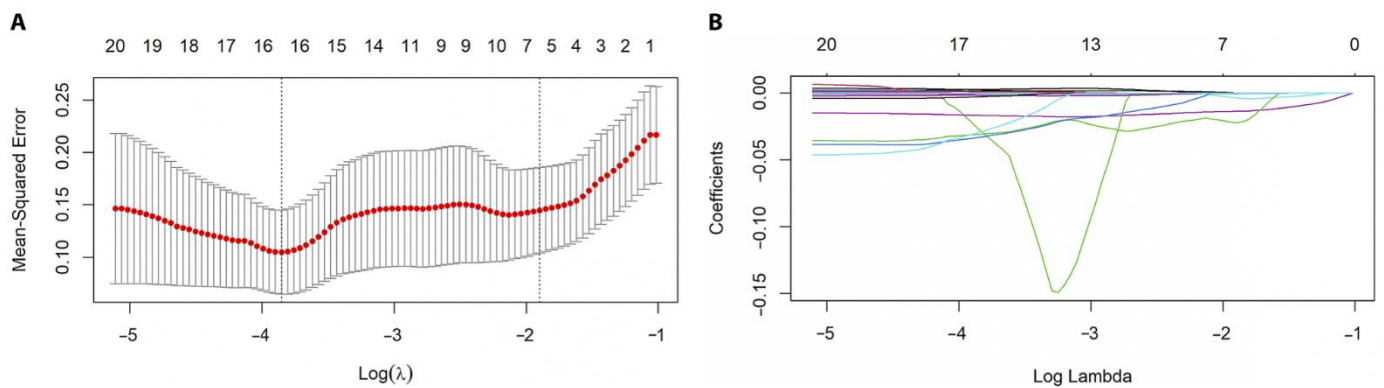


**Figure 5.** Least Absolute Shrinkage and Selection Operator (LASSO) regression analysis. (A) The minimum mean squared error was achieved and 16 hub genes were identified at the best  $\lambda = 0.022$ . (B) When the  $\log(\lambda)$  value increased, all coefficients shrunk precisely to zero.

### 3.4.2. Correlation Analysis

We first investigated the proportion of immune cells using the CIBERSORT and TIMER algorithms (Supplementary Table S5). Figure 6A (CIBERSORT) and 6B (TIMER) indicate that each immune cell type was not significantly different between the low- and high-TB groups.

Spearman's method was used to identify the correlation between hub genes and immune cell types generated by CIBERSORT and TIMER (Figure 7). Eleven (Figure 7A) and five genes (Figure 7B) were significantly correlated with CIBERSORT and TIMER immune cells, respectively. Finally, the Venn diagram (Figure 7C) identified four candidate genes (overlapping genes), including one upregulated (*FCGR3B*) and three downregulated (*ROBO2*, *OPRL1*, and *NR4A2*) genes.

### 3.5. PPI Network Analysis

A network of 106 IR-DEGs was constructed using STRING and displayed in Cytoscape (Figure 8). The confidence score was 0.4 and the PPI enrichment  $p$  value was  $1 \times 10^{-16}$ . *FCGR3B*, *ROBO2*, *OPRL1*, and *NR4A2* were significantly enriched in seven KEGG pathways and 51 GO terms (Tables 2, 3, S6 and S7). Interestingly, *FCGR3B* was the hub gene for the natural-killer-cell-mediated cytotoxicity and phagosome pathways.

**Table 2.** Kyoto Encyclopedia of Genes and Genomes pathways interacted with four candidate genes.

| Term Name | Description                               | Genes | FDR                   |
|-----------|---|-------|-----------------------|
| hsa04650  | Natural killer cell mediated cytotoxicity | 11    | $9.34 \times 10^{-9}$ |
| hsa04080  | Neuroactive ligand-receptor interaction   | 12    | $4.44 \times 10^{-6}$ |
| hsa05152  | Tuberculosis                              | 8     | $5.28 \times 10^{-5}$ |
| hsa04380  | Osteoclast differentiation                | 7     | $6.87 \times 10^{-5}$ |
| hsa04360  | Axon guidance                             | 7     | $4.20 \times 10^{-4}$ |
| hsa04145  | Phagosome                                 | 6     | $9.10 \times 10^{-4}$ |
| hsa05150  | Staphylococcus aureus infection           | 5     | $9.10 \times 10^{-4}$ |

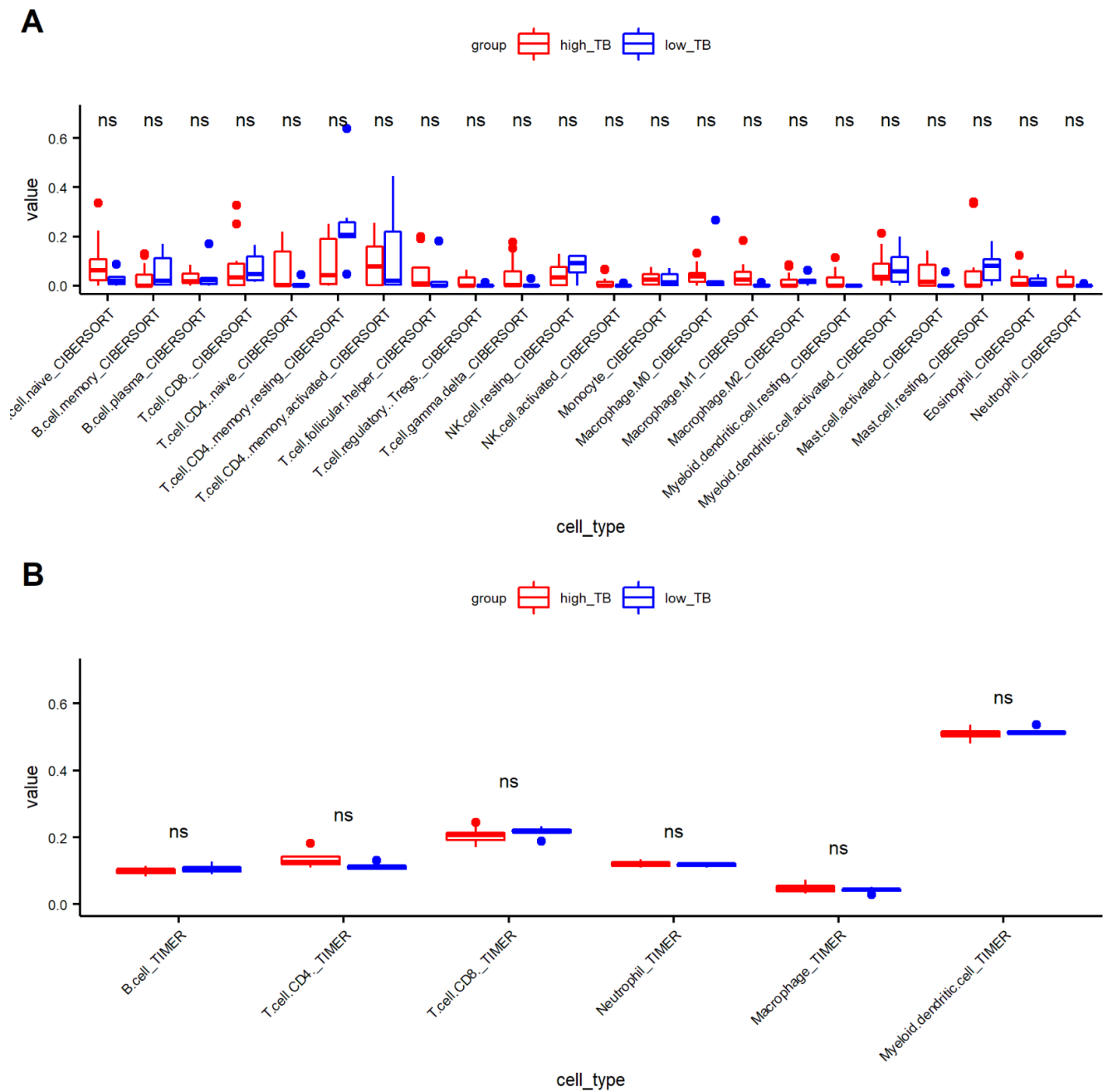


**Figure 6.** Distribution of immune cell types between high- and low-tumor budding (TB). (A) CIBERSORT and (B)TIMER. (NK.cell, natural killer cell; ns, non significant).



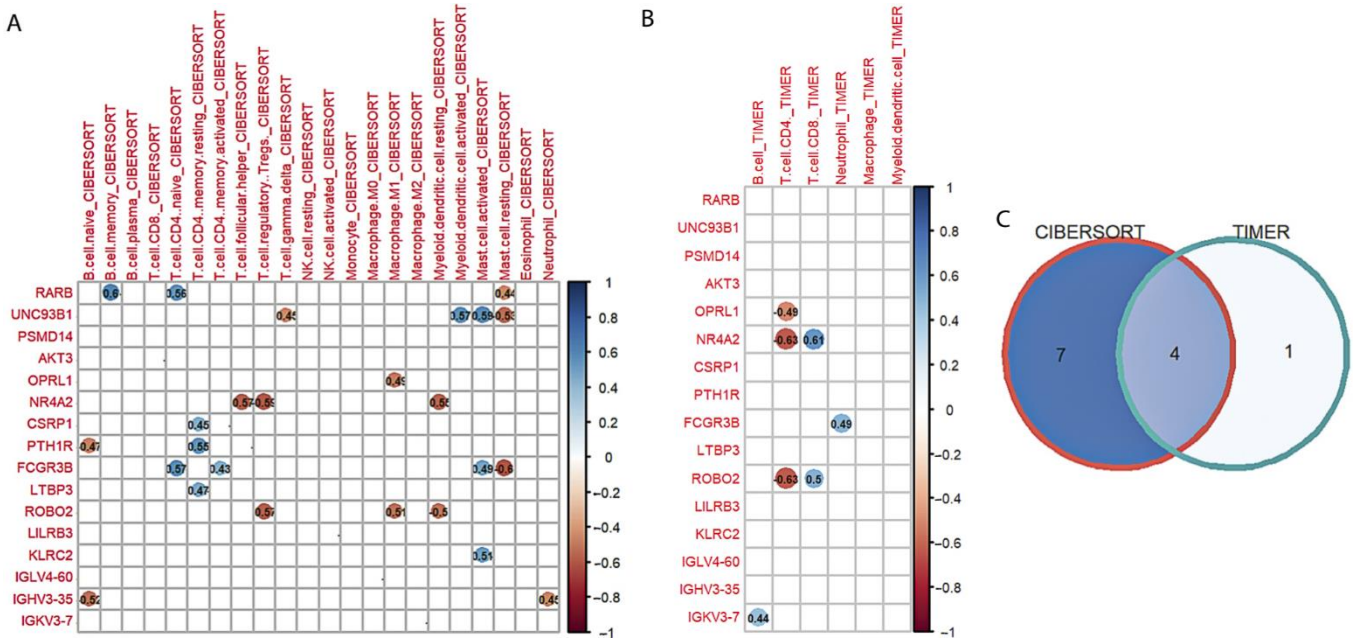


**Figure 7.** Identification of candidate genes. (A) Correlation between 16 hub genes and CIBERSORT immune cell types. (B) Correlation between 16 hub genes and TIMER immune cell types. (C) Venn diagram of overlap genes. Red and blue circles represent the significant negative and positive correlation, respectively. (NK.cell, natural killer cell).

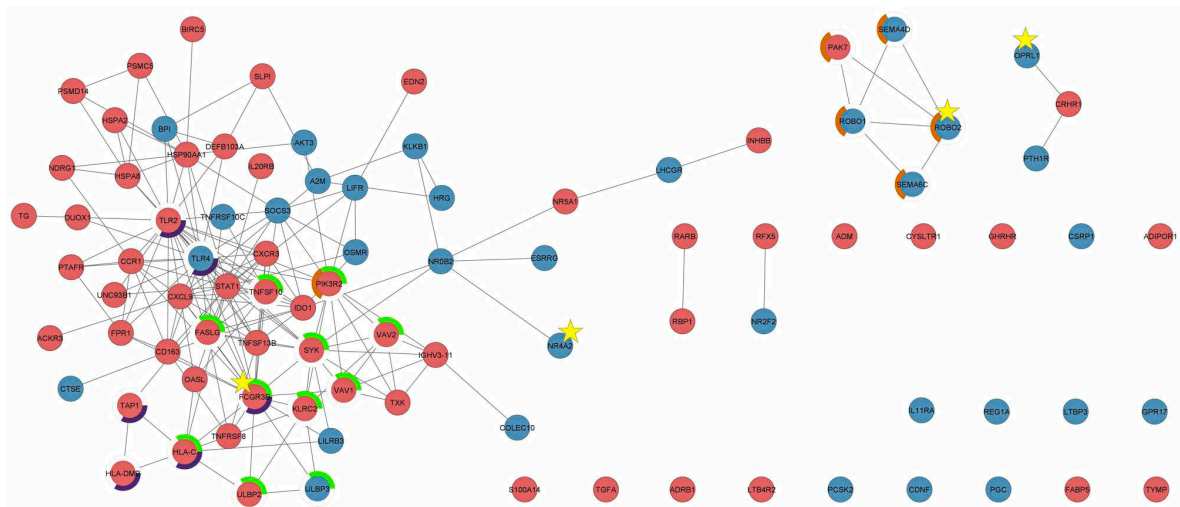


**Figure 8.** Protein–protein interaction network of 106 immune-related differentially expressed genes. “Red” and “blue” represent the upregulated and downregulated genes, respectively. The gray lines (edges) indicate interactions between connected nodes. Star highlights the candidate gene. The green, purple, and orange circles represent the natural-killer-cell-mediated cytotoxicity, phagosome, and axon guidance pathway, respectively.

**Table 3.** Top 10 Gene Ontology (GO) terms interacted with four candidate genes.

| Category           | Term Name  | Description                                    | Count | FDR                    |
|--------------------|------------|--|-------|------------------------|
| GO-BP <sup>1</sup> | GO:0007165 | Signal transduction                            | 73    | $1.60 \times 10^{-23}$ |
| GO-BP              | GO:0006955 | Immune response                                | 42    | $2.38 \times 10^{-18}$ |
| GO-MF <sup>2</sup> | GO:0005102 | Signaling receptor binding                     | 41    | $2.81 \times 10^{-17}$ |
| GO-MF              | GO:0038023 | Signaling receptor activity                    | 36    | $3.54 \times 10^{-14}$ |
| GO-BP              | GO:0050776 | Regulation of immune response                  | 27    | $4.30 \times 10^{-12}$ |
| GO-BP              | GO:0048584 | Positive regulation of response to stimulus    | 40    | $8.52 \times 10^{-12}$ |
| GO-CC <sup>3</sup> | GO:0009986 | Cell surface                                   | 26    | $1.49 \times 10^{-11}$ |
| GO-BP              | GO:0006935 | Chemotaxis                                     | 20    | $5.35 \times 10^{-10}$ |
| GO-MF              | GO:0008528 | G protein-coupled peptide receptor activity    | 12    | $6.22 \times 10^{-9}$  |
| GO-BP              | GO:0051239 | Regulation of multicellular organismal process | 42    | $2.67 \times 10^{-8}$  |

<sup>1</sup> GO-BP, Gene Ontology biological process; <sup>2</sup> GO-MF, Gene Ontology molecular function; <sup>3</sup> GO-CC, Gene Ontology cellular component.

### 3.6. ROC Curve and Survival Analysis

ROC analysis was conducted to investigate the accuracy of the four candidate genes as diagnostic biomarkers for low- and high-TB levels. The area under the curve (AUC) of *FCGR3B*, *ROBO2*, *OPRL1*, and *NR4A2* was 81.7%, 92.2%, 82.2%, and 94.4%, respectively (Figure 9). However, only the *FCGR3B* expression level significantly differed in OS ( $p = 0.0016$ ; Figure 10).

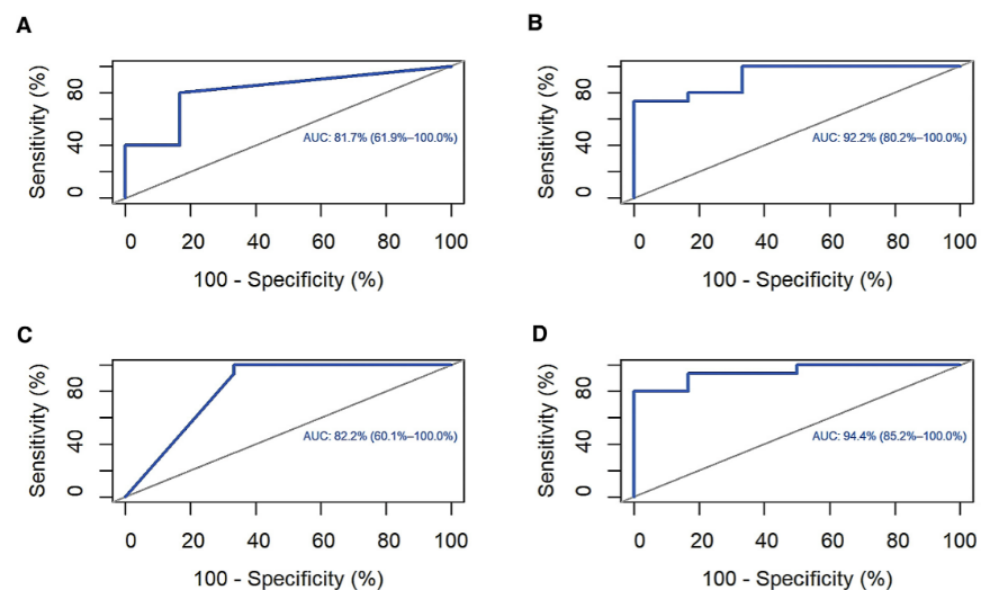


**Figure 9.** Receiver operating characteristic (ROC) curve analysis. (A) Fc region  $\gamma$  receptor III-B (*FCGR3B*), (B) roundabout guidance receptor 2 (*ROBO2*), (C) opioid-related nociceptin receptor 1 (*OPRL1*), and (D) nuclear receptor subfamily 4 group A member 2 (*NR4A2*).

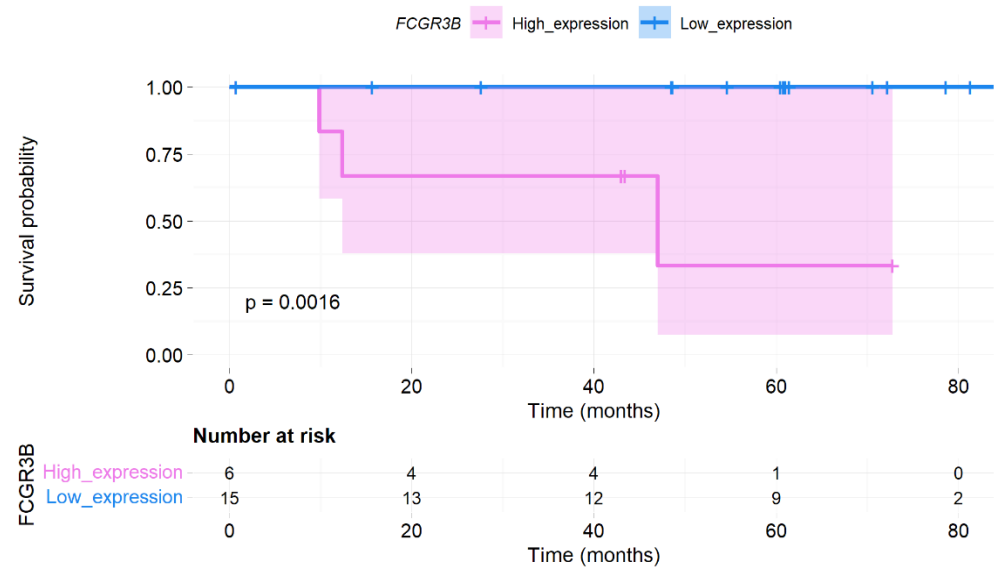


**Figure 10.** Survival analysis. Kaplan–Meier plot for Fc region  $\gamma$  receptor III-B (FCGR3B) expression level in overall survival.

#### 4. Discussion

Recent studies have noted the high correlation between TB status and cancer progression [5–7,16]. Because tumor progression results from the interaction between tumor cells and the TME, insights into biological TB can provide potential tools for cancer management [5]. However, the relationship between tumor bud and TME, particularly TIME, has been unclear. Therefore, this is one of the first studies identifying the transcriptomic immune profiles of TB in CC.

In this study, 1464 DEGs were obtained by comparing the gene expression between high- and low-TB groups. By intersecting these DEGs and 2483 public immune-related genes, we selected 106 IR-DEGs. Functional analysis showed that these IR-DEGs mainly involve innate immune pathways, such as the natural killer (NK)-cell-mediated cytotoxicity, cytokine–cytokine receptor interaction, chemokine signaling, JAK-STAT, and Toll-like receptor signaling pathways. Most current reports consider CD8+T cells, FOXP3+T cells, and CD68+ macrophages to be the primary innate immune response in the tumor microenvironment [5,36]. Nevertheless, NK also plays a crucial role in the TIME. For example, Garcia-Iglesias et al. reported that NK-activating receptors and the cytotoxic activity of NK cells significantly decrease in high-grade squamous intraepithelial lesions and CC [37].

To investigate the candidate genes from the 106 IR-DEGs, multiple analyses were conducted. Briefly, the LASSO regression algorithm was implemented and 16 hub genes were identified. Then, the correlation between hub genes and immune cell types was analyzed to select candidate genes. Finally, one upregulated (*FCGR3B*) and three downregulated (*ROBO2*, *OPRL1*, and *NR4A2*) genes were identified. PPI network analysis revealed the functional insights of the four candidate genes in TB status.

First, high *FCGR3B* expression induces TB progression by suppressing NK-cell-mediated cytotoxicity and phagocytosis. *FCGR3B* encodes a low-affinity immunoglobulin  $\gamma$  Fc region receptor III-B protein (Fc $\gamma$ RIIIb), a member of the IgG Fc receptor family (Fc $\gamma$ Rs) [38]. Fc $\gamma$ Rs play crucial roles in cancer immunotherapy via antibody-dependent cellular cytotoxicity and phagocytosis [38].

Previous studies have reported six human Fc $\gamma$ Rs (Fc $\gamma$ RI/CD64, Fc $\gamma$ RIIa/CD32a, Fc $\gamma$ RIIb/CD32b, Fc $\gamma$ RIIc/CD32c, Fc $\gamma$ RIIIa/CD16a, and Fc $\gamma$ RIIIb/CD16b) [39,40]. *Fc $\gamma$ RIIIb/CD16b* is mainly expressed by neutrophils and also negatively regulates neutrophil activities in the TIME [39,41]. Even though the interaction between neutrophils and NK cells in TIME is unclear, neutrophils can enhance NK-derived interferon (IFN) $\gamma$  to suppress tumor progression and angiogenesis [42–44]. In addition, this study

found that the *FCGR3B* expression level accurately predicts the TB status (AUC = 81.7%) and patient survival (high expression causes poor prognosis in OS,  $p = 0.0016$ ). Therefore, *FCGR3B* may be a novel biomarker for high TB in CC.

Second, low *ROBO2* expression may lead to a high-TB status through the axon guidance signaling pathway. The *ROBO2* gene encodes roundabout guidance receptor two protein that functions as an axon guidance receptor by binding to secreted SLIT ligands [45–47]. The ROBO family is frequently downregulated in several cancers and considered an anti-oncogene [48]. The SLIT/ROBO signaling can inhibit tumor progression through some mechanisms, such as preventing cell migration and angiogenesis, enhancing cell–cell adhesion, and blocking endothelial cell proliferation [49]. Interestingly, this signaling can regulate macrophage immune responses by inducing cytoskeletal changes in macrophages, preventing macrophage spreading and inhibiting macropinocytosis [50]. Although the *ROBO2* expression level in this study was not significantly related to patient survival prognosis because of the small sample size, *ROBO2* can still be a promising marker for predicting TB status (AUC = 92.2%).

Lastly, *NR4A2* (nuclear receptor subfamily 4 group A member 2) and *OPRL1* (opioid-related nociceptin receptor 1) were significantly enriched in several important biological processes, such as signal transduction, signaling receptor binding, signaling receptor activity, cell–cell signaling, and regulation of cell death. These findings suggest that *OPRL1* and *NR4A2* downregulation may enhance TB progression in CC. In other words, these genes function as tumor suppressors. With substantial diagnostic accuracy from ROC analysis, *OPRL1* and *NR4A2* are promising candidates for predicting TB status. Although there are several conflicting data regarding the role of *NR4A2* and *OPRL1* in cancer, our results are in accordance with current observations: *NR4A2* can trans-activate Foxp3, involved in the differentiation, maintenance, and function of regulatory T cells, and plays a significant role in cancer cell development and survival [51–53]. Furthermore, Inamoto et al. reported that *NR4A2* is a tumor suppressor in human bladder cancer tissues [51]. Regarding *OPRL1*, it belongs to the  $A\gamma$  family of G protein-coupled receptors, which are involved in various diseases, including cancer [54,55]. Bedini et al. revealed that *OPRL1* acts as a tumor inhibitor in U87 glioblastoma cells by blocking lipopolysaccharide [56]. In addition, *OPRL1* can activate markers on the surface of T cells, enhance CD4<sup>+</sup> T and CD8<sup>+</sup> T-cell proliferation, and alter cytokine secretion, which is closely involved in tumor progression [57].

This study lacks experimental validation. Therefore, further studies should be conducted to clarify the mechanisms of these candidate genes in TB progression.

## 5. Conclusions

Four immune-related genes (one upregulated (*FCGR3B*) and three downregulated (*ROBO2*, *OPRL1*, and *NR4A2*) genes) that can impact TB formation and development were detected through a multiple-step analysis. These genes may be potential biomarkers for replacing TB status to stratify CC patients. Furthermore, they can provide novel ideas for immune-targeted therapeutic strategies in the future.

**Supplementary Materials:** The following supporting information can be downloaded at: <https://www.mdpi.com/article/10.3390/genes13081405/s1>. Table S1: Significant differentially expressed genes between the low- and high-tumor-budding group. Table S2: Immune-related differentially expressed genes. Table S3: Kyoto Encyclopedia of Genes and Genomes (KEGG) pathways. Table S4: Gene Ontology (GO) terms. Table S5: Proportion of immune cell types using the TIMER and CIBERSORT algorithms. Table S6: GO-term of 106 IR-DEGs with STRING enrichment. Table S7: GO-term of 106 IR-DEGs with STRING enrichment. Figure S1: Representative microscopic features of high tumor budding (TB) histology.

**Author Contributions:** Conceptualization, T.M.L., N.J.-Y.P., H.S.H. and G.O.C.; Formal analysis, T.M.L., H.D.T.N., E.L., D.L. and J.C.; Investigation, N.J.-Y.P., H.S.H. and G.O.C.; Methodology, T.M.L., H.D.T.N., E.L., N.J.-Y.P., H.S.H. and G.O.C.; Project administration, N.J.-Y.P., H.S.H. and G.O.C.; Writing—original draft, T.M.L.; Writing—review and editing, H.D.T.N., E.L., D.L., Y.S.C., J.C., N.J.-Y.P., H.S.H. and G.O.C. All authors have read and agreed to the published version of the manuscript.

**Funding:** This research was funded by the Biomedical Research Institute grant from Kyungpook National University Hospital (2020).

**Institutional Review Board Statement:** This study was approved by the Institutional Review Board of Kyungpook National University Chilgok Hospital (KNUCH 2020–03-011).

**Informed Consent Statement:** Patient consent was waived due to the retrospective study.

**Data Availability Statement:** Not applicable.

**Conflicts of Interest:** The authors declare no conflict of interest.

## References

1. Ferlay, J.; Ervik, M.; Lam, F.; Colombet, M.; Mery, L.; Piñeros, M.; Znaor, A.; Soerjomataram, I.; Bray, F. *Global Cancer Observatory: Cancer Today*; International Agency for Research on Cancer: Lyon, France, 2020. Available online: <https://gco.iarc.fr/today/about#references> (accessed on 28 March 2022).
2. Huang, B.; Cai, J.; Xu, X.; Guo, S.; Wang, Z. High-Grade Tumor Budding Stratifies Early-Stage Cervical Cancer with Recurrence Risk. *PLoS ONE* **2016**, *11*, e0166311. [[CrossRef](#)] [[PubMed](#)]
3. Satabongkoch, N.; Khunamornpong, S.; Pongsuvareeyakul, T.; Settakorn, J.; Sukpan, K.; Soongkhaw, A.; Intaraphet, S.; Suprasert, P.; Siriaunkgul, S. Prognostic Value of Tumor Budding in Early-Stage Cervical Adenocarcinomas. *Asian Pac. J. Cancer Prev.* **2017**, *18*, 1717. [[CrossRef](#)] [[PubMed](#)]
4. Chong, G.O.; Jee-Young Park, N.; Han, H.S.; Cho, J.; Kim, M.G.; Choi, Y.; Yeo, J.Y.; Lee, Y.H.; Hong, D.G.; Park, J.Y. Intratumoral Budding: A Novel Prognostic Biomarker for Tumor Recurrence and a Potential Predictor of Nodal Metastasis in Uterine Cervical Cancer. *Eur. J. Surg. Oncol.* **2021**, *47*, 3182–3187. [[CrossRef](#)]
5. Lugli, A.; Zlobec, I.; Berger, M.D.; Kirsch, R.; Nagtegaal, I.D. Tumour Budding in Solid Cancers. *Nat. Rev. Clin. Oncol.* **2021**, *18*, 101–115. [[CrossRef](#)] [[PubMed](#)]
6. Ailia, M.J.; Thakur, N.; Chong, Y.; Yim, K. Tumor Budding in Gynecologic Cancer as a Marker for Poor Survival: A Systematic Review and Meta-Analysis of the Perspectives of Epithelial–Mesenchymal Transition. *Cancers* **2022**, *14*, 1431. [[CrossRef](#)] [[PubMed](#)]
7. Park, J.Y.; Chong, G.O.; Park, J.Y.; Chung, D.; Lee, Y.H.; Lee, H.J.; Hong, D.G.; Han, H.S.; Lee, Y.S. Tumor Budding in Cervical Cancer as a Prognostic Factor and Its Possible Role as an Additional Intermediate-Risk Factor. *Gynecol. Oncol.* **2020**, *159*, 157–163. [[CrossRef](#)]
8. Jin, M.Z.; Jin, W.L. The Updated Landscape of Tumor Microenvironment and Drug Repurposing. *Signal Transduct. Target. Ther.* **2020**, *5*, 166. [[CrossRef](#)]
9. Balkwill, F.R.; Capasso, M.; Hagemann, T. The Tumor Microenvironment at a Glance. *J. Cell Sci.* **2012**, *125*, 5591–5596. [[CrossRef](#)]
10. Schiavoni, G.; Gabriele, L.; Mattei, F. The Tumor Microenvironment: A Pitch for Multiple Players. *Front. Oncol.* **2013**, *3*, 90. [[CrossRef](#)]
11. Vesely, M.D.; Kershaw, M.H.; Schreiber, R.D.; Smyth, M.J. Natural Innate and Adaptive Immunity to Cancer. *Annu. Rev. Immunol.* **2011**, *29*, 235–271. [[CrossRef](#)]
12. Nearchou, I.P.; Lillard, K.; Gavriel, C.G.; Ueno, H.; Harrison, D.J.; Caie, P.D. Automated Analysis of Lymphocytic Infiltration, Tumor Budding, and Their Spatial Relationship Improves Prognostic Accuracy in Colorectal Cancer. *Cancer Immunol. Res.* **2019**, *7*, 609–620. [[CrossRef](#)] [[PubMed](#)]
13. Dawson, H.; Christe, L.; Eichmann, M.; Reinhard, S.; Zlobec, I.; Blank, A.; Lugli, A. Tumour Budding/T Cell Infiltrates in Colorectal Cancer: Proposal of a Novel Combined Score. *Histopathology* **2020**, *76*, 572–580. [[CrossRef](#)]
14. Pecorelli, S.; Zigliani, L.; Odicino, F. Revised FIGO Staging for Carcinoma of the Cervix. *Int. J. Gynecol. Obstet.* **2009**, *105*, 107–108. [[CrossRef](#)] [[PubMed](#)]
15. Lugli, A.; Kirsch, R.; Ajioka, Y.; Bosman, F.; Cathomas, G.; Dawson, H.; El Zimaity, H.; Fléjou, J.F.; Hansen, T.P.; Hartmann, A.; et al. Recommendations for Reporting Tumor Budding in Colorectal Cancer Based on the International Tumor Budding Consensus Conference (ITBCC) 2016. *Mod. Pathol.* **2017**, *30*, 1299–1311. [[CrossRef](#)]
16. Park, J.Y.; Hong, D.G.; Chong, G.O.; Park, J.Y. Tumor Budding Is a Valuable Diagnostic Parameter in Prediction of Disease Progression of Endometrial Endometrioid Carcinoma. *Pathol. Oncol. Res.* **2019**, *25*, 723–730. [[CrossRef](#)] [[PubMed](#)]
17. Bolger, A.M.; Lohse, M.; Usadel, B. Trimmomatic: A Flexible Trimmer for Illumina Sequence Data. *Bioinformatics* **2014**, *30*, 2114–2120. [[CrossRef](#)]
18. Andrews, S. FastQC: A Quality Control Tool for High Throughput Sequence Data. Available online: <https://www.bioinformatics.babraham.ac.uk/projects/fastqc/> (accessed on 8 September 2021).

19. Bray, N.L.; Pimentel, H.; Melsted, P.; Pachter, L. Near-Optimal Probabilistic RNA-Seq Quantification. *Nat. Biotechnol.* **2016**, *34*, 525–527. [[CrossRef](#)]
20. Love, M.I.; Huber, W.; Anders, S. Moderated Estimation of Fold Change and Dispersion for RNA-Seq Data with DESeq2. *Genome Biol.* **2014**, *15*, 1–21. [[CrossRef](#)]
21. Wickham, H. *Ggplot2: Elegant Graphics for Data Analysis*; Springer: New York, NY, USA, 2016; ISBN 978-3-319-24277-4.
22. Bhattacharya, S.; Dunn, P.; Thomas, C.G.; Smith, B.; Schaefer, H.; Chen, J.; Hu, Z.; Zalocusky, K.A.; Shankar, R.D.; Shen-Orr, S.S.; et al. ImmPort, toward Repurposing of Open Access Immunological Assay Data for Translational and Clinical Research. *Sci. Data* **2018**, *5*, 180015. [[CrossRef](#)]
23. Huang, D.W.; Sherman, B.T.; Lempicki, R.A. Systematic and Integrative Analysis of Large Gene Lists Using DAVID Bioinformatics Resources. *Nat. Protoc.* **2009**, *4*, 44–57. [[CrossRef](#)]
24. Li, B.; Severson, E.; Pignon, J.C.; Zhao, H.; Li, T.; Novak, J.; Jiang, P.; Shen, H.; Aster, J.C.; Rodig, S.; et al. Comprehensive Analyses of Tumor Immunity: Implications for Cancer Immunotherapy. *Genome Biol.* **2016**, *17*, 1–16. [[CrossRef](#)] [[PubMed](#)]
25. Sturm, G.; Finotello, F.; Petitprez, F.; Zhang, J.D.; Baumbach, J.; Fridman, W.H.; List, M.; Aneichyk, T. Comprehensive Evaluation of Transcriptome-Based Cell-Type Quantification Methods for Immuno-Oncology. *Bioinformatics* **2019**, *35*, i436–i445. [[CrossRef](#)]
26. Newman, A.M.; Steen, C.B.; Liu, C.L.; Gentles, A.J.; Chaudhuri, A.A.; Scherer, F.; Khodadoust, M.S.; Esfahani, M.S.; Luca, B.A.; Steiner, D.; et al. Determining Cell Type Abundance and Expression from Bulk Tissues with Digital Cytometry. *Nat. Biotechnol.* **2019**, *37*, 773–782. [[CrossRef](#)] [[PubMed](#)]
27. Kassambara, A. Ggpubr: “ggplot2” Based Publication Ready Plots. R Package Version 0.4.0. 2020. Available online: <https://CRAN.R-project.org/package=ggpubr> (accessed on 10 July 2022).
28. Friedman, J.; Hastie, T.; Tibshirani, R. Regularization Paths for Generalized Linear Models via Coordinate Descent. *J. Stat. Softw.* **2010**, *33*, 1–22. [[CrossRef](#)] [[PubMed](#)]
29. Wei, T.; Simko, V. R Package “corrplot”: Visualization of a Correlation Matrix (Version 0.92). 2021. Available online: <https://github.com/taiyun/corrplot> (accessed on 10 July 2022).
30. Szklarczyk, D.; Gable, A.L.; Nastou, K.C.; Lyon, D.; Kirsch, R.; Pyysalo, S.; Doncheva, N.T.; Legeay, M.; Fang, T.; Bork, P.; et al. The STRING Database in 2021: Customizable Protein–Protein Networks, and Functional Characterization of User-Uploaded Gene/Measurement Sets. *Nucleic Acids Res.* **2021**, *49*, D605. [[CrossRef](#)]
31. Shannon, P.; Markiel, A.; Ozier, O.; Baliga, N.S.; Wang, J.T.; Ramage, D.; Amin, N.; Schwikowski, B.; Ideker, T. Cytoscape: A Software Environment for Integrated Models of Biomolecular Interaction Networks. *Genome Res.* **2003**, *13*, 2498–2504. [[CrossRef](#)] [[PubMed](#)]
32. Robin, X.; Turck, N.; Hainard, A.; Tiberti, N.; Lisacek, F.; Sanchez, J.C.; Müller, M. PROC: An Open-Source Package for R and S+ to Analyze and Compare ROC Curves. *BMC Bioinform.* **2011**, *12*, 77. [[CrossRef](#)]
33. Kassambara, A.; Kosinski, M.; Biece, P. survminer: Drawing Survival Curves Using “ggplot2”. R Package Version 0.4.9. 2021. Available online: <https://CRAN.R-project.org/package=survminer> (accessed on 10 July 2022).
34. Therneau, T. A Package for Survival Analysis in R. R Package Version 3.3-1. 2022. Available online: <https://CRAN.R-project.org/package=survival> (accessed on 10 July 2022).
35. Therneau, M.T.; Grambsch, M.P. *Modeling Survival Data: Extending the Cox Model*; Springer: New York, NY, USA, 2000; ISBN 978-1-4757-3294-8.
36. Wartenberg, M.; Cebin, S.; Zlobec, I.; Vassella, E.; Eppenberger-Castori, S.; Terracciano, L.; Eichmann, M.D.; Worni, M.; Gloor, B.; Perren, A.; et al. Integrated Genomic and Immunophenotypic Classification of Pancreatic Cancer Reveals Three Distinct Subtypes with Prognostic/ Predictive Significance. *Clin. Cancer Res.* **2018**, *24*, 4444–4454. [[CrossRef](#)]
37. Garcia-Iglesias, T.; del Toro-Arreola, A.; Albarran-Somoza, B.; del Toro-Arreola, S.; Sanchez-Hernandez, P.E.; Ramirez-Dueñas, M.; Balderas-Peña, L.M.A.; Bravo-Cuellar, A.; Ortiz-Lazareno, P.C.; Daneri-Navarro, A. Low NKp30, NKp46 and NKG2D Expression and Reduced Cytotoxic Activity on NK Cells in Cervical Cancer and Precursor Lesions. *BMC Cancer* **2009**, *9*, 186. [[CrossRef](#)]
38. Junker, F.; Gordon, J.; Qureshi, O. Fc Gamma Receptors and Their Role in Antigen Uptake, Presentation, and T Cell Activation. *Front. Immunol.* **2020**, *11*, 1393. [[CrossRef](#)]
39. Patel, K.R.; Roberts, J.T.; Barb, A.W. Multiple Variables at the Leukocyte Cell Surface Impact Fc  $\gamma$  Receptor-Dependent Mechanisms. *Front. Immunol.* **2019**, *10*, 223. [[CrossRef](#)]
40. Barb, A.W. Fc  $\gamma$  Receptor Compositional Heterogeneity: Considerations for Immunotherapy Development. *J. Biol. Chem* **2021**, *296*, 100057. [[CrossRef](#)]
41. Treffers, L.W.; van Houdt, M.; Bruggeman, C.W.; Heineke, M.H.; Zhao, X.W.; van der Heijden, J.; Nagelkerke, S.Q.; Verkuijlen, P.J.J.H.; Geissler, J.; Lissenberg-Thunnissen, S.; et al. Fc $\gamma$ RIIIb Restricts Antibody-Dependent Destruction of Cancer Cells by Human Neutrophils. *Front. Immunol.* **2019**, *10*, 1–13. [[CrossRef](#)]
42. Palano, M.T.; Gallazzi, M.; Cucchiara, M.; de Lerma Barbaro, A.; Gallo, D.; Bassani, B.; Bruno, A.; Mortara, L. Neutrophil and Natural Killer Cell Interactions in Cancers: Dangerous Liaisons Instructing Immunosuppression and Angiogenesis. *Vaccines* **2021**, *9*, 1488. [[CrossRef](#)]
43. Shimasaki, N.; Jain, A.; Campana, D. NK Cells for Cancer Immunotherapy. *Nat. Rev. Drug Discov.* **2020**, *19*, 200–218. [[CrossRef](#)]
44. Bassani, B.; Baci, D.; Gallazzi, M.; Poggi, A.; Bruno, A.; Mortara, L. Natural Killer Cells as Key Players of Tumor Progression and Angiogenesis: Old and Novel Tools to Divert Their Pro-Tumor Activities into Potent Anti-Tumor Effects. *Cancers* **2019**, *11*, 461. [[CrossRef](#)] [[PubMed](#)]

45. Mehlen, P.; Delloye-Bourgeois, C.; Chédotal, A. Novel Roles for Slits and Netrins: Axon Guidance Cues as Anticancer Targets? *Nat. Rev. Cancer* **2011**, *11*, 188–197. [[CrossRef](#)]
46. Tessier-Lavigne, M.; Goodman, C.S. The Molecular Biology of Axon Guidance. *J. S. Nye R. Kopan Curro Bioi* **1995**, *210*, 27. [[CrossRef](#)]
47. Kidd, T.; Bland, K.S.; Goodman, C.S. Slit Is the Midline Repellent for the Robo Receptor in *Drosophila*. *Cell* **1999**, *96*, 785–794. [[CrossRef](#)]
48. Mitra, S.; Mazumder-Indra, D.; Mondal, R.K.; Basu, P.S.; Roy, A.; Roychoudhury, S.; Panda, C.K. Inactivation of SLIT2-ROBO1/2 Pathway in Premalignant Lesions of Uterine Cervix: Clinical and Prognostic Significances. *PLoS ONE* **2012**, *7*, e38342. [[CrossRef](#)] [[PubMed](#)]
49. Ballard, M.S.; Hinck, L. A Roundabout Way to Cancer. *Adv. Cancer Res.* **2012**, *114*, 187. [[CrossRef](#)] [[PubMed](#)]
50. Bhosle, V.K.; Mukherjee, T.; Huang, Y.W.; Patel, S.; Pang, B.W.F.; Liu, G.Y.; Glogauer, M.; Wu, J.Y.; Philpott, D.J.; Grinstein, S.; et al. SLIT2/ROBO1-Signaling Inhibits Macropinocytosis by Opposing Cortical Cytoskeletal Remodeling. *Nat. Commun.* **2020**, *11*, 1–17. [[CrossRef](#)] [[PubMed](#)]
51. Inamoto, T.; Czerniak, B.A.; Dinney, C.P.; Kamat, A.M. Cytoplasmic Mislocalization of the Orphan Nuclear Receptor Nurr1 Is a Prognostic Factor in Bladder Cancer. *Cancer* **2010**, *116*, 340–346. [[CrossRef](#)] [[PubMed](#)]
52. Han, Y.F.; Cao, G.W. Role of Nuclear Receptor NR4A2 in Gastrointestinal Inflammation and Cancers. *World J. Gastroenterol.* **2012**, *18*, 6865. [[CrossRef](#)] [[PubMed](#)]
53. Ke, N.; Claassen, G.; Yu, D.H.; Albers, A.; Fan, W.; Tan, P.; Grifman, M.; Hu, X.; DeFife, K.; Nguy, V.; et al. Nuclear Hormone Receptor NR4A2 Is Involved in Cell Transformation and Apoptosis. *Cancer Res.* **2004**, *64*, 8208–8212. [[CrossRef](#)] [[PubMed](#)]
54. Ishikawa, R.; Imai, A.; Mima, M.; Yamada, S.; Takeuchi, K.; Mochizuki, D.; Shinmura, D.; Kita, J.Y.; Nakagawa, T.; Kurokawa, T.; et al. Novel Prognostic Value and Potential Utility of Opioid Receptor Gene Methylation in Liquid Biopsy for Oral Cavity Cancer. *Curr. Probl. Cancer* **2022**, *46*, 100834. [[CrossRef](#)]
55. Lappano, R.; Maggiolini, M. G Protein-Coupled Receptors: Novel Targets for Drug Discovery in Cancer. *Nat. Rev. Drug Discov.* **2011**, *10*, 47–60. [[CrossRef](#)]
56. Bedini, A.; Baiula, M.; Vincelli, G.; Formaggio, F.; Lombardi, S.; Caprini, M.; Spampinato, S. Nociceptin/Orphanin FQ Antagonizes Lipopolysaccharide-Stimulated Proliferation, Migration and Inflammatory Signaling in Human Glioblastoma U87 Cells. *Biochem. Pharmacol.* **2017**, *140*, 89–104. [[CrossRef](#)]
57. Waits, P.S.; Purcell, W.M.; Fulford, A.J.; McLeod, J.D. Nociceptin/Orphanin FQ Modulates Human T Cell Function in Vitro. *J. Neuroimmunol.* **2004**, *149*, 110–120. [[CrossRef](#)]